Geomechanics and Engineering, *Vol. 38, No. 1 (2024) 57-68*
https://doi.org/10.12989/gae.2024.38.1.057

Finite element analysis of shallow buried tunnel subjected to traffic loading by damage mechanics theory

Mohammadreza Tameh*

Department of Civil and Environmental Engineering, University of Kashan, Kashan, Iran

(*Received April 5, 2023, Revised June 27, 2024, Accepted June 28, 2024*)

Abstract. Tunnels offer myriad benefits for modern countries, and understanding their behavior under loads is critical. This paper analyzes and evaluates the damage to buried horseshoe tunnels under soil pressure and traffic loading. To achieve this, a numerical model of this type of tunnel is first created using ABAQUS software. Then, fracture mechanics theory is applied to investigate the fracture and damage of the horseshoe tunnel. The numerical analysis is based on the damage plasticity model of concrete, which describes the inelastic behavior of concrete in tension and compression. In addition, the reinforcing steel is modeled using the bilinear plasticity model. Damage contours, stress contours, and maximum displacements illustrate how and where traffic loading alters the response of the horseshoe tunnel. Based on the results, the fracture mechanism proceeded as follows: initially, damage started at the center of the tunnel bottom, followed by the formation of damage and micro-cracks at the corners of the tunnel. Eventually, the damage reached the top of the concrete arch with increasing loading. Therefore, in the design of this tunnel, these critical areas should be reinforced more to prevent cracking.

Keywords: buried tunnel; cracking analysis; damage mechanics; finite-element analysis; soil and traffic loads

1. Introduction

With the massive bloom in urbanization over the past many years, there has been a decrease in the availability of land for the construction of roads and railways. As an alternative to reduce the congestion on the surface, underground transit tunnels have been built in many countries. They have proven to benefit society both in economic and environmental aspects. Shallow buried Tunnels are mostly designed for conventional load conditions including ground pressure and seismic, as evident from many published studies (Bendjebbas *et al.* 2016, Hashash *et al.* 2001, Jiang and Yin 2012, Singh *et al.* 2017, Yu *et al.* 2017).

Road tunnels, either buried, underground, under rivers or even subsea tunnels, are usually constructed as an important part of modern highway networks to shorten the travel time within or between cities, reduce transportation costs, and improve traffic capacity (Cui *et al.* 2015, Wang *et al.* 2020, Wang *et al.* 2020). Based on open reports and literature, Fig. 1 summarizes the total number of tunnels in the world. By 2019, China has built 19,067 road tunnels with the total mileage of 18966.6 km (MTPRC, 2020). By the end of 2016, the total length of tunnels in service in China exceeded 14,120 km, the length of railway tunnels under construction was about 9,300 km, and the length of railway tunnels under design and planning was about 10,400 km (Wang and Zhao 2006, Zhao and Li 2018). By 2020, the total number of tunnels in service in China is expected to reach 17,000, with a total length of more than 20,000 km ; by 2030, the total length will exceed 30,000 km (Zhao and Li 2018). Also, the total length of tunnels in Germany in 2023, 2022, and 2021 are 30,622 km, 47,801 km, and 47,365, respectively (Haack 2003). With the foreseeable growth of transportation demand, road tunnels will be more intensively constructed worldwide and play increasingly vital roles in the transportation systems by virtue of its great advantage in overcoming physical barrier and minimizing local environment impact (Bassan 2015).

In most engineering works, the service life of structure is a significant problem that should consider in the design process. In this situation, the ability of a designer to predict damage conditions of the structure under negative factors is an essential issue. For example, unpredicted damages of tunnels that are related to unpredicted fractures in concrete and reinforcing steel bars cause significant economical and safety damages and prevent transit. Also, in the design of this type of structures, fracture predicting is a determinative factor and unpredicted fractures in important structures such as shallow buried tunnels may have catastrophic effects. Therefore, it is necessary to include all negative factors in the design process of tunnels.

One of these negative factors that would not be ignore, is traffic loading. Nowadays, the population of the countries is increasing and this leads to using more cars on the roads and more services for people. Shallow buried tunnels as underground public transit systems should stay in a serviceable state over time and any damage to them could result in heavy causalities and economic loss. This requires a strengthening of shallow buried tunnels against possible traffic overloading on the roads. This in turn necessitates a thorough understanding of the structural behavior of shallow buried tunnels under traffic loading. In other words,

*Corresponding author, Master Engineer
E-mail: Mohammadreza.tameh@gmail.com

ISSN: 2005-307X (Print), 2092-6219 (Online)

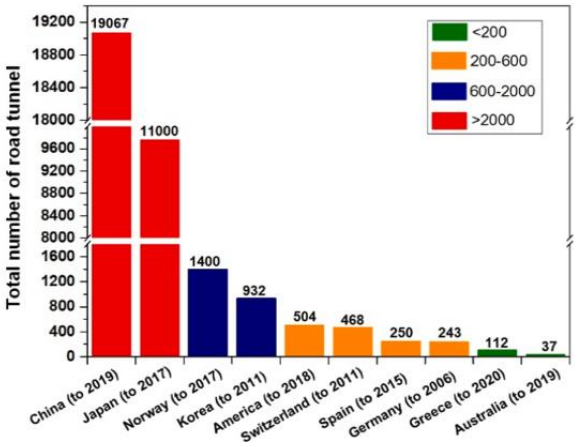

Fig. 1 The total number of road tunnels

tunnels placed close to roads and railways are expected to experience additional traffic loading; consequently, tunnels may be subjected to increased deformations that can lead to failure. Therefore, it is essential to evaluate the effects of traffic loads on the response of shallow buried tunnels. So, this paper analyzes and evaluates the damage of buried horseshoe tunnels under soil pressure and traffic loading by damage mechanics theory, which has not been previously explored in the literature.

1.1 Damage mechanics theory

Annually, the fracture problem has many financial and physical costs in different countries. At the beginning of twenty century, the scientistic looking to this issue was started and created new fields in mechanics science with the name of fracture mechanics. Generally, two different methods are used for modeling of fracture processes of quasi-brittle materials:1) fracture mechanics, 2) damage mechanics.

In the present world, many structures are seemingly healthy and flawless. But, in micro-scale viewpoint, they have micro-cracks, micro-holes and a variety of disadvantages. They propagate in the structure, connect together and cause the final fracture of the structure. Therefore, many structures may do not have any visible damage on the macro-scale, but they have many micro-cracks and micro-holes in the micro-scale. Fracture mechanics science considers the starting and growth process of micro-cracks as a discontinuous phenomenon. In other words, fracture mechanics theory is commonly applied in structural integrity assessments, failure analysis, and the design of materials and structures to prevent catastrophic failure due to crack propagation. Therefore, the study of crack initiation, propagation, and failure within materials is the goal of this theory. In this way, it provides predictions of how cracks propagate and whether they will lead to catastrophic failure, often through the analysis of stress intensity factors and fracture toughness. Also, fracture mechanics typically focuses on quasi-static or dynamic loading conditions and is less concerned with the time-dependent aspects of damage accumulation. For instance, Elastic-Plastic Fracture Mechanics (EPFM) uses strain energy fields or opening displacement near the crack tips to determine the conditions for crack growth.

In contrast, damage mechanics is a practical engineering method in continuum mechanics used to predict the behavior of materials under complex loading conditions or long-term degradation. It encompasses the consideration of material damage from initiation to fracture without relying on a microscopic description. The theory of damage mechanics finds applications in various fields, including structural engineering, materials science, geomechanics, and biomechanics. Damage mechanics aims to elucidate how a material's properties change as it undergoes damage, including phenomena like micro-cracking, yielding, or stiffness degradation. This theory emphasizes the progressive accumulation of damage, which can lead to critical levels of damage or deterioration in material properties under loading conditions. Much of the research in damage mechanics utilizes state variables to depict the impact of damage on stiffness and the remaining life of the material. These state variables may be directly measurable, such as crack density, or inferred from their influence on certain macroscopic properties like stiffness, coefficient of thermal expansion, and remaining life (Struik, 1978).

Nevertheless, damage mechanics can predict the reduction of characteristics and material properties due to micro-crack effects. As a concrete tunnel is constructed into the soil, it undergoes soil pressure from laterals, bottom, and top regions. This loads on the tunnel can create damage on the tunnel. When a traffic load is added to the system, the conditions become more complex. Therefore, in this study damage mechanics is adopted to evaluate the responses of concrete tunnel under soil pressure and traffic load.

1.2 Damage types

(Kachanov 1986) was the first person that allocated a continuous variable to damage density. This variable contains the fundamental relationships for growth. These relationships are written based on stress and strain. They are used to structural calculations in order to predict the growth of macro-cracks. (Voyiadjis and Kattan 2005) have classified the damage types into three groups:

1. Flexible damage: when significant plastic deformations happen simultaneously with damage growth in space, it is named "flexible damage". Fundamental relationships were presented by (Lemaitre 1984, 1986), (Lemaitre and Dufailly 1987) and (Kattan and Voyiadjis 1990, Voyiadjis and Kattan, 1990). In these relationships, the elastic and elasto-plastic effects were considered.

2. Damage due to fatigue: When a material is subjected to cyclic loading, over time, plastic strain accumulates in the structure. As a result, damage occurs due to these strains, known as 'damage due to fatigue.' This damage is classified into two categories: high-cycle fatigue and low-cycle fatigue. Basic relationships for this damage was presented by (LEMAITRE, 1971).

3. Damage due to creep: when a metal is subjected to loading in high temperature (for example, a temperature above the melting point), the plastic strain is associated with a viscosity property that results in the material being

deformed under constant stress. Over time, with the development of these visco-plastic strains in the space, the particle separation happens in the material that causes damage in space. This type of damage is called "damage due to creep". (Hult 1974), (Lemaitre and Chaboche 1975) and (Hult 1974) presented the primary relationships of this problem.

1.3 Researches on the failure mechanism of tunnel

In 1986, (Lemaitre 1986) used a summary of the work done 15 years ago to apply the behavior of crack by using the damage mechanics theory. Also, (Lemaitre and Dufailly 1987) raised eight different experimental methods to measure of damage. Although the damage is non-identical, but it can be assumed to be identical in many quasi-brittle materials with a good approximation. In the identical and non-identical states, the damage variable is scaler and higher-order tensor, respectively.

Some works have been conducted about the failure mechanism of tunnel. For instance,(Yang *et al*. 2016) studied tunnel roof failure mechanisms in homogeneous and layered soils. The results show that, in layered soils, the total height and the width on the layered position of possible collapsing block increase, and the width of the falling block on the tunnel roof decreases when only the upper soil's dilatancy coefficient decreases. Moreover, (Yoo 2016) investigated the deformation behavior of tunnels crossing a weak zone. A three-dimensional finite element model was adopted that allows realistic modeling of the tunnel. The results indicate that the effectiveness of the absolute displacement monitoring data as early warning indicators depends strongly on the spatial characteristics of the weak zone.

(Nikadat and Marji 2016) evaluated the effects of two basic geometric factors influencing tunnel behavior in a jointed rock mass on the stress distribution around the tunnel. This numerical analysis revealed that both the dip angle and spacing of joints have important influences on stress distribution on tunnel walls. Also, (Huang *et al*. 2018) investigated the failure mechanism of tunnel roof with the upper bound theorem of limit analysis. It is shown that the material parameters of initial cohesion, nonlinear coefficient and unit weight have significant influence on the potential range of tunnel collapse. (Chen *et al.* 2019) proposed a new improved failure mechanism to evaluate the stability of the tunnel and introduced the critical places. (Zaid 2021) conducted a simulation in order to understand the behavior of rock tunnel under static loading condition.

(Nikadat *et al.* 2015) examined how the behavior of large discontinuities (faults) affects a jointed medium surrounding rectangular tunnels. The results demonstrated that the dip angle of these discontinuities plays a significant role in determining the stress distribution around the tunnels. Furthermore, an increase in the dip angle of discontinuities located in the tunnel's roof leads to a decrease in tensile stress in that region. The greatest tensile stress occurs at the intersection of a 60° fault and the tunnel roof, while the highest compressive stress is observed at the intersection of a 30° fault and the tunnel wall. Moreover, corners within rectangular tunnels cause dilation

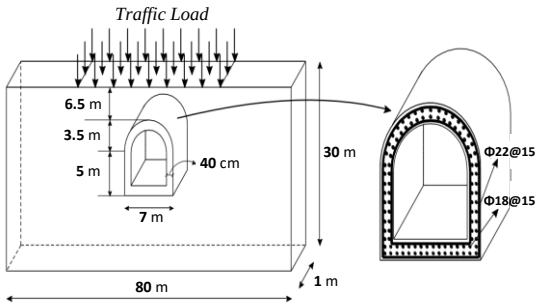

Fig. 2 Model geometry

perpendicular to the orientation of in-situ stress, resulting in a higher concentration of stress in the walls compared to the roof and floor. (Abdollahipour *et al*. 2016) presented a numerical formulation and implementation for the poroelastic displacement discontinuity method (DDM). Additionally, they introduced a scheme for crack propagation in crack propagation problems, demonstrated through an example. This allows the code to track crack propagation over both time and space. Using experimental techniques alongside the extended finite element method, (Haeri *et al.* 2020) explored how the joint number and its angular variations affect both the compressive behavior of joint bridge regions and their tensile strength. Results underscored that the failure process is primarily dictated joint number and joint angularities. Furthermore, the strength of specimens declines with an escalation in both joint number and joint angularities.

Nevertheless, the research on the failure mechanism of horseshoe-shape tunnels under the traffic load and soil pressure has not been seen in the literature. Therefore, this article applies damage analysis to horseshoe tunnels under soil pressure and traffic load using damage mechanics theory. To carry out the numerical analysis, ABAQUS software is used. The damage conditions of the reinforced horseshoe tunnel in the soil are investigated using the damage plasticity model, which describes the complete inelastic behavior of concrete in tension and compression. Finally, a traffic damage assessment is conducted to identify the most vulnerable and most robust parts of the tunnel against traffic loading.

2.Geometry and finite element model of tunnel

A typical transit tunnel with horseshoe cross section of height 8.5 m and width 7 m is considered in this study. A cover depth of 6.5 m is taken on top of the tunnel. The tunnel is made of concrete with normal strength of 30 MPa, elasticity modulus of 23.9 GPa, poisson's ratio of 0.2 and weight density of 2500 kg/m3. The thickness of the tunnel lining is assumed to be 400 mm along with double reinforcement using 18-mm diameter and 22-mm Fe 420 bars (Schwer 2014). The longitudinal and hoop reinforcement bars are placed with a center-to-center spacing of 150 mm and also concrete cover is 50 mm (Fig. 2). Also reinforcing steel with a yield strength of 420 MPa, elasticity modulus of 200 GPa, Poisson's ratio of 0.3 and weight density of 7850 kg/m^3 was used.

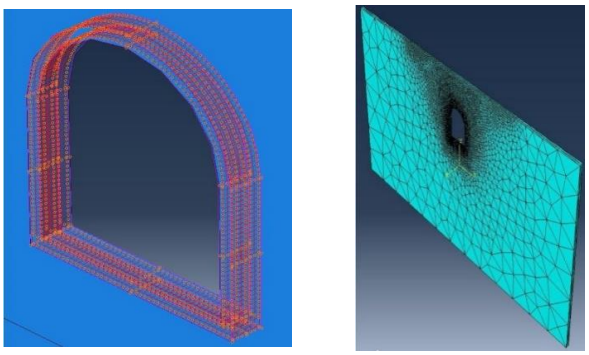

(a) Reinforcing steel modeling (b) Tetrahedral elements

Fig. 3 Numerical modeling details

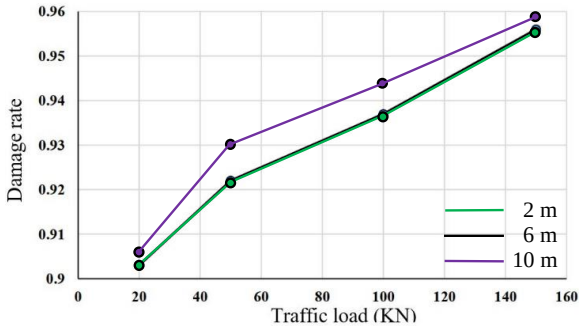

Fig. 4 Sensitivity of the damage rate in the tunnel to the level of mesh refinement at the boundary

In 3D space to reduce the computational time and memory consumption, a soil medium with dimension of 80x30 meters and thickness of 1 meter was created in plain-strain condition. The behavior of the unbounded soil domain is simulated by assigning 3D viscous dashpots to the external boundaries of the soil model, following the formulation proposed by Lysmer and Kuhlemeyer (1969). Moreover, the bottom of the model is fixed in all directions. In numerical modeling, three-dimensional element with ten nodes (tetrahedral) is used for meshing of the soil that it is demonstrated in Fig. 3(b) (51270 elements and 83348 nodes). Furthermore, it is important to determine the appropriate level of mesh refinement in the soil domain. To do this, a convergence study is carried out with three element sizes of 2, 6, and 10 m for boundary elements. The soil domain dimensions are the same for all three meshes (i.e., 80.0 m " 1.0 m " 30.0 m), and the size of the elements decreases as they get closer to the tunnel. The models are subjected to the same traffic loads. The resulting damage rates are presented in Fig. 4, showing almost no difference between the results of the first and second levels of mesh refinement. Finally, the element size of 6 m gave sufficiently accurate results. The mesh size around the tunnel was considered small enough (small enough to capture the wave propagation accurately). In order to simulate the reinforcing steel, element T3D3 is used in ABAQUS software that this element is a three-dimensional trust element with three nodes. In this numerical modeling, also to define the interface between concrete and steel, the embedded region constraint used to constrain the degrees of freedom of steel element with surrounding concrete elements. The value of fractional exterior tolerance is selected of 0.05. Also, the sliding of reinforcing steel is ignored. Fig. 3(a) presents the modeling and configuration of reinforcing steel in the model. The traffic live load in this study has been considered as a uniform pressure (Bryden *et al.* 2015, Kraus *et al* 2014, Trickey and Moore 2007, Yoo *et al.* 1999).

3. Materials models

3.1 Concrete

Three different types of constitutive equations are considered for concrete: 1) smeared crack constitutive model, 2) brittle crack constitutive model 3) damage plastic constitutive model. In this article, the damage plastic constitutive model is used and this model will be explained below. The damage plastic constitutive model formulated based on studies of (Lubliner *et al.* 1989) and (Lee and Fenves 1998). This constitutive model is applicable for states that concrete and others of quasi-brittle materials are under uniform, cyclic and dynamic loading in the low hydrostatic pressure. The principal fracture mechanisms involve cracking under tension and fracture under compression. Generally, this model requires three groups of parameters: plasticity parameters, uniaxial compressive and tensile stress-strain curves of concrete, and damage parameters for compression and tension. Each of these cases will be described below.

3.1.1 Plasticity parameters

These kinds of parameters include the plastic flow rule and yield function. The plastic flow rule is the hyperbolic Drucker-Prager function. The general criterion for this function is as follows:

$$G = \sqrt{(\varepsilon\sigma_{t0}tan\varphi)^2 + q^2} - Ptan\varphi \quad (1)$$

Where ε = eccentricity; φ = dilation angle; σ_{t0} = uniaxial tensile stress at failure; P= hydrostatic pressure stress and q = Von-Mises equivalent effective stress. The Von-Mises equivalent effective stress can be expressed as

$$q = \sqrt{\frac{3}{2}S.S} \quad (2)$$

Where S is the effective stress deviator, defined as

$$S = \sigma + PI \quad (3)$$

Where σ is the effective stress and P is the hydrostatic pressure stress and can be calculated as follow

$$P = -{}^{1}/_{3}\, trace(\sigma) \quad (4)$$

The yield function expressed with the yield function of (Lubliner *et al.* 1989) and suggested changing by (Lee and Fenves 1998). The yield function criterion is defined as

$$F = \frac{1}{1-\alpha}[q - 3\alpha p + \beta(\varepsilon^{pl})(\hat{\sigma}_{max}) - \gamma(-\hat{\sigma}_{max})] - \sigma_c(\varepsilon^{pl}) = 0 \quad (5)$$

Where the value of α, β and γ is calculated below.

$$\alpha = [(^{\sigma_{b0}}/_{\sigma_{c0}}) - 1]/[2(^{\sigma_{b0}}/_{\sigma_{c0}}) - 1] \quad (6)$$

$$\beta = \frac{\sigma_c(\varepsilon_c^{pl})}{\sigma_t(\varepsilon_t^{pl})}(1-\alpha) - (1+\alpha)0 \quad (7)$$

$$\gamma = \frac{3(1-K_c)}{2K_c - 1} \quad (8)$$

In the Eqs. (5)-(8) the parameter $\hat{\sigma}_{max}$ is the maximum of available stress and $^{\sigma_{b0}}/_{\sigma_{c0}}$ is the ratio of biaxial maximum compressive stress to the axial maximum compressive stress that the value of this parameter based on the suggestion of the ABAQUS software is 1.16. Kc is a determinative parameter for the transversal sectional shape of yield surface that also the value of this parameter based on the suggestion of the ABAQUS software is 0.667. $\sigma_c(\varepsilon_c^{pl})$ and $\sigma_t(\varepsilon_t^{pl})$ are the compressive and tensile axial stresses in available plastic strain.

3.1.2 Axial compressive and tensile stress-strain curve of concrete

The axial stress-strain curve of concrete introduces by the user as the inelastic stress-strain in the software. In order to simulate the tensile behavior of concrete completely, young modulus E_0, tensile stress σ_t, cracking strain $\varepsilon_t^{\sim ck}$ and tensile damage parameter d_t are needed. Concrete cracking strain is calculated as

$$\varepsilon_t^{\sim ck} = \varepsilon_t - \varepsilon_{ot}^{el} \quad (9)$$

Where $\varepsilon_{ot}^{el} = {}^{\sigma_t}/_{E_0}$ = elastic strain associated with non-damaged materials in tension and ε_t = total tensile strain. ABAQUS uses the plastic strain to evaluate the validation of the damage curve. The negative and descending value of tensile plastic strain shows the unacceptable damage curve and causes an error before performing the analysis.

$$\varepsilon_t^{\sim pl} = \varepsilon_t^{\sim ck} - \frac{d}{1-d_t}\frac{\sigma_t}{E_0} \quad (10)$$

In order to simulate the compressive behavior of reinforced concrete completely in ABAQUS, compressive stress σ_c, inelastic strain $\varepsilon_c^{\sim in}$ and compressive damage parameter d_c are needed. Therefore, the total strain should be changed to an inelastic strain as below.

$$\varepsilon_c^{\sim in} = \varepsilon_c - \varepsilon_{oc}^{el} \quad (11)$$

Where $\varepsilon_{oc}^{el} = {}^{\sigma_c}/_{E_0}$ = elastic strain associated with non-damaged materials in compression and ε_c = total compressive strain. In the pressure, should also be taken to ensure that the plastic strain values calculated by the following equation are neither negative nor decreasing with increasing stress (Wahalathantri *et al.* 2011).

$$\varepsilon_c^{\sim pl} = \varepsilon_c^{\sim in} - \frac{d_c}{1-d_c}\frac{\sigma_c}{E_0} \quad (12)$$

3.1.3 Damage parameters in compression and tension

Damage in solid materials is the growth and creation of micro-cracks and micro-holes that on the micro-scale and macro-scale are discontinuous and continuum, respectively. Damage mechanics defined based on the effective stress concept by (Kachanov 1986) and has been used in many practical and engineering works (Fig. 5). In the same way, in this study also this concept is used.

The ideal curve of stress-strain of concrete in compression and tension is shown in Fig. 6. According to this figure, the slope of the curve up to the initial yield stress σ_{c0}, is equal to initial young modulus, E_0. When the concrete is unloaded from any point on the strain-softening branch, the unloading slope of the curve due to the cracking and crushing in the concrete will be less than E_0; even it will have a lower value than the initial value. The compressive damage parameter d_c is used to express the stiffness reduction of concrete during compressive unloading. In these conditions, the unloading slope of the curve is obtained from multiplying $1 - d_c$ in the initial young modulus. d_c can be zero corresponding to completely non-damaged state and one corresponding to completely damaged state. Usually, to prevent numerical instabilities, the value of d_c is not chosen more than 0.99. Also, according to Fig. 6 can be stated that there are similar definitions of tension except that in the tensile behavior, the stress-strain curve is linear to the peak point of stress. After that, a softening branch is observed, similar to a straight line for some materials such as concrete.

The following equations use in order to determination of damage parameters in compression and tension. (Birtel and Mark 2006) believe that the determination of damage parameters in compression and tension is related to

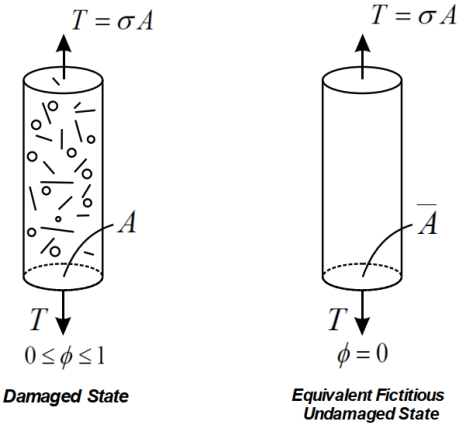

Fig. 5 Isotropic damage in axial tension state (based on effective stress concept)(Voyiadjis and Kattan 2005)

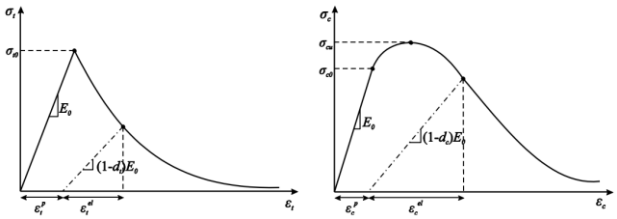

Fig. 6 The ideal curve of concrete in tension and compression (Systemes 2011)

corresponding plastic strains that are calculated from the following equations.

$$d_c = 1 - \frac{\sigma_c E_c^{-1}}{\varepsilon_c^{pl}\left(\frac{1}{b_c} - 1\right) + \sigma_c E_c^{-1}} \quad (13)$$

$$d_t = 1 - \frac{\sigma_t E_c^{-1}}{\varepsilon_t^{pl}\left(\frac{1}{b_t} - 1\right) + \sigma_t E_c^{-1}} \quad (14)$$

Where E_c=elasticity modulus of concrete, σ_c= concrete compressive stress, σ_t = concrete tensional stress, ε_c^{pl} = compressive plastic strain of concrete, ε_t^{pl}= tensional plastic strain of concrete, b_c= constant parameter in compression (suggested value=0.7) and b_t = constant parameter in tension (suggested value=0.1).

3.2 Reinforcement

The stress-strain relationship of reinforcing steel in concrete is shown in Fig. 7. This relationship is valid for both longitudinal and transverse reinforcement. The following equations mathematically convey the stress-strain relationship of reinforcing steel in concrete (Pilkey and Pilkey 2005).

$$f_s = E_s \varepsilon_s \quad \varepsilon_s \le \varepsilon_n \quad (15)$$

$$f_s = f_y\left[(0.91 - 2B) + (0.02 + 0.25B)\frac{\varepsilon_s}{\varepsilon_y}\right]\left(1 - \frac{2 - \alpha_2/45^\circ}{1000\rho}\right) \quad ; \varepsilon_s > \varepsilon_n \quad (16)$$

$$(\varepsilon_n = \varepsilon_y(0.93 - 2B)\left(1 - \frac{2 - \alpha_2/45^\circ}{1000\rho}\right) \quad (17)$$

Where in Eq. (16), the coefficient $[(0.91 - 2B) + (0.02 + 0.25B)\left(\varepsilon_s/\varepsilon_y\right)]$ is the average steel stress in post-yield branch and coefficient $[1 - \frac{2 - \frac{\alpha_2}{45^\circ}}{1000\rho}]$ is related to reinforcing steel torsion in the crack. When α_2 is equal to 45 degrees, the torsion coefficient is equal to $[\frac{1}{1000\rho}]$ and when α_2 is equal to 90 degrees, the torsion coefficient is equal to one.

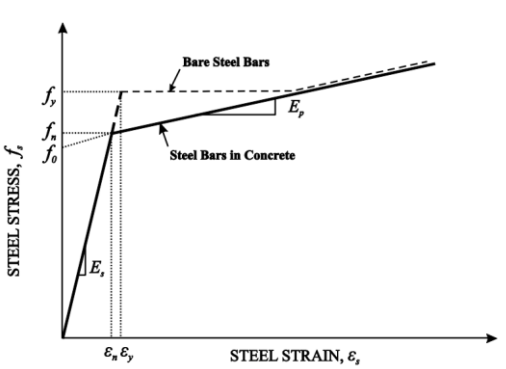

Fig. 7 Bilinear model of reinforcing steel in concrete

3.3 Soil

The thickness of the soil layer is 30 m and a dense engineering bedrock with a shear wave velocity of 800 m/s is located below the uniform sand layer. It should be noted that in the numerical model, soil sites are classified based on the average shear wave velocity of the top 30 m of soil layers. However, the maximum depth of 30 m in the conventional numerical site investigations generally did not extend down to the stiff bedrock with V_S more than 800 m/s. Investigations on the influence of the bedrock stiffness in numerical simulations of the seismic site response show that an increase in stiffness of bedrock cannot significantly affect the overall seismic response of a site and the site response is mostly governed by the upper soil layers (Falcone *et al.* 2020). The simplified numerical models provide a quantification of the surface ground motion modification with an error generally equal to ±10% with respect to the realistic conditions (Falcone *et al.* 2020). The finite element soil domain was discretized with three-dimensional element with ten nodes (tetrahedral). Soil density and Poisson's ratios of soil deposit were considered to be 2200 kg/m^3 and 0.3, respectively. It is assumed that the shear modulus (G_Z) for the site was varied with depth (Z) as Eq. (18), where G_h denotes shear modulus at depth h, and n represents the dimensionless shear modulus exponent. This common equation is considered for the homogeneous soil type C in the present study and the values of parameters n, h, and G_h were assumed to be 0.7, 15 m, and 182 MPa, respectively. The average shear wave velocity at the top 30 m of the soil is computed by Eq. (19), according to Eurocode 8 (Acun 2012); h_i and V_{si} stand for the thickness (in meters) and the shear wave velocity of the i-th formation.

$$G_z = G_h(\frac{Z}{h})^n \quad (18)$$

$$V_{s,30} = \frac{30}{\sum_{i=1,N}\frac{h_i}{V_{si}}} \quad (19)$$

4. Results and discussions

Fig. 8 presents the horizontal displacement of the soil and horseshoe tunnel under soil pressure and traffic loading at the final stage. It is noteworthy that, This contour is the size of deformation in space ($U = \sqrt{U_x^2 + U_y^2 + U_z^2}$). In the soil, the displacement increases with decreasing the depth (from the surface). In the far regions from the tunnel, the soil deformation is uniform in the X direction, but getting closer to the tunnel becomes non-uniform. This is due that, the stiffness of the concrete is much more than the soil, so the deformation of the soil around the tunnel is less than in the upper area (about 0.3 mm). The displacement is zero at the model's base and equal 18.4 mm at the soil surface. This displacement is dependent on the amount of stiffness of soil and traffic loads. With consideration of the high damage to the tunnel, this amount of displacement is logical.

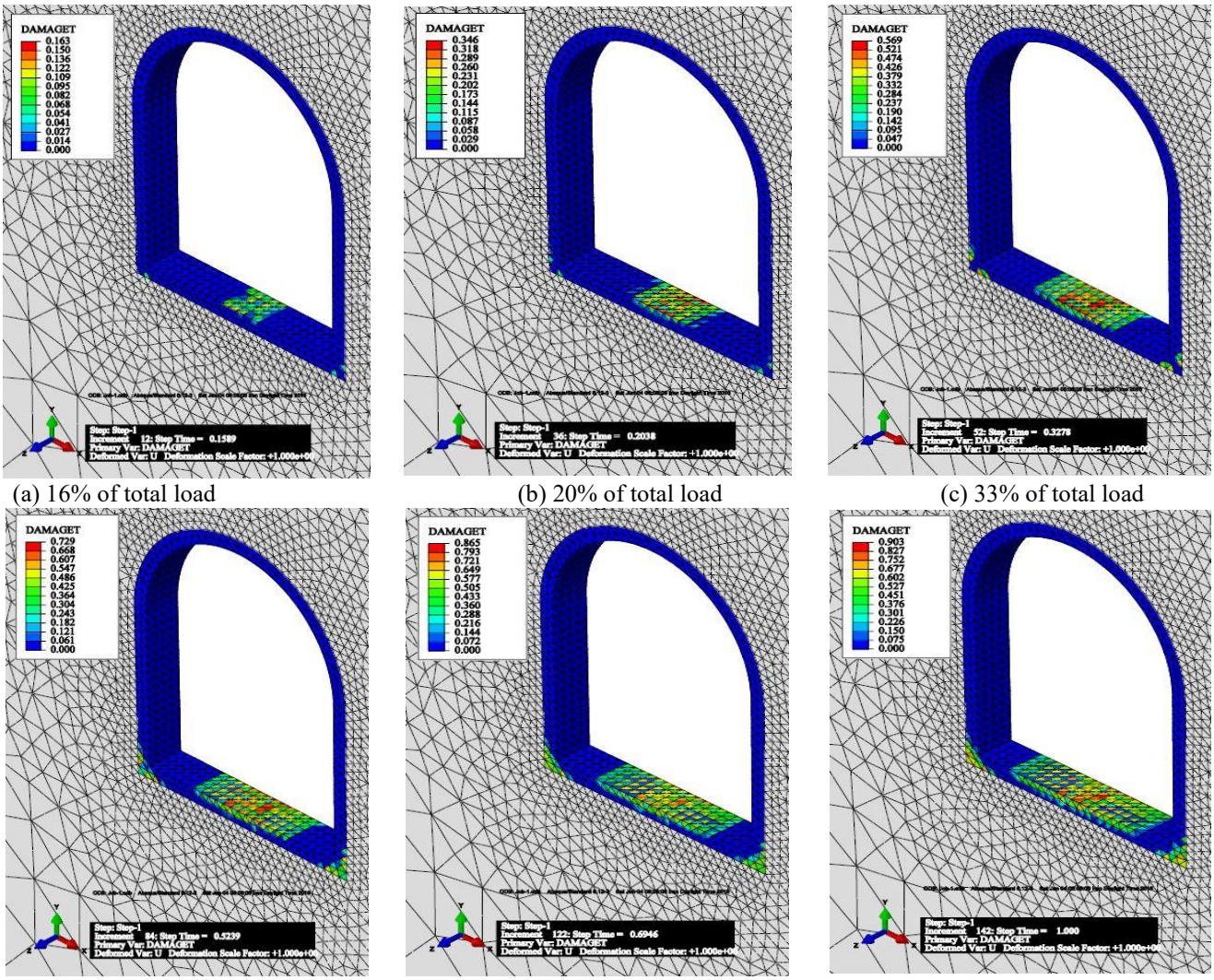

(a) 16% of total load (b) 20% of total load (c) 33% of total load

(d) 52% of total load (e) 69% of total load (f) 100% of total load

Fig. 9 Damage contours of concrete in different stages of traffic loading

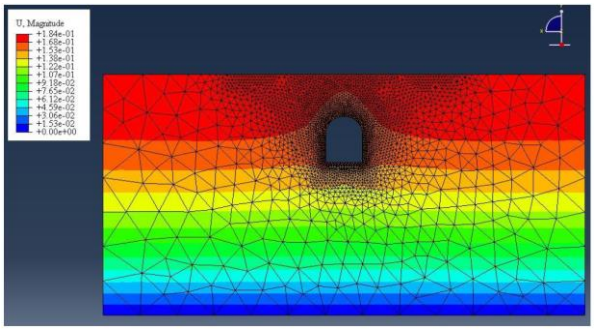

Fig. 8 Final displacements of the concrete box and soil

Fig. 9 shows the damage contour in concrete in the different stages of traffic loading. It should be said that, zero damage is equal to healthy material and unit damage is equivalent to completely damaged material (complete cracking). It can be seen that at each stage of loading, the maximum damage happens in the center of the tunnel bottom. This is due to the geometrical shape of the tunnel, which transfer the loads to the base of the tunnel. First, the damage occurs in the center of the tunnel bottom, with increasing traffic loading, damage in concrete extends to the corners of the horseshoe tunnel.

According to Fig. 9(a) to 9(f), when the traffic load increase, more volume (in width and height) of the central and corner concrete regions became damaged. Finally, in the final stage of traffic loading (Fig. 9(f)), the maximum damage in the center of the tunnel reaches 0.9 and this value indicates that the concrete has completely cracked and lost its strength. On the other hand, the damage value in the corners of the tunnel is less than in the central region (about 0.6). Nevertheless, the most vulnerable and critical part against soil pressure and traffic load is the central areas of the bottom of the horseshoe tunnel. So, this part of the tunnel needs more attention in the design process. For instance, designers can use more reinforcement in this region or use better concrete with higher mechanical properties in order to prevent creating a crack.

Also, Fig. 10 illustrates the damage contours of concrete in different stages of loading plus deformation with a scale factor of 50. According to these deformations, it can be

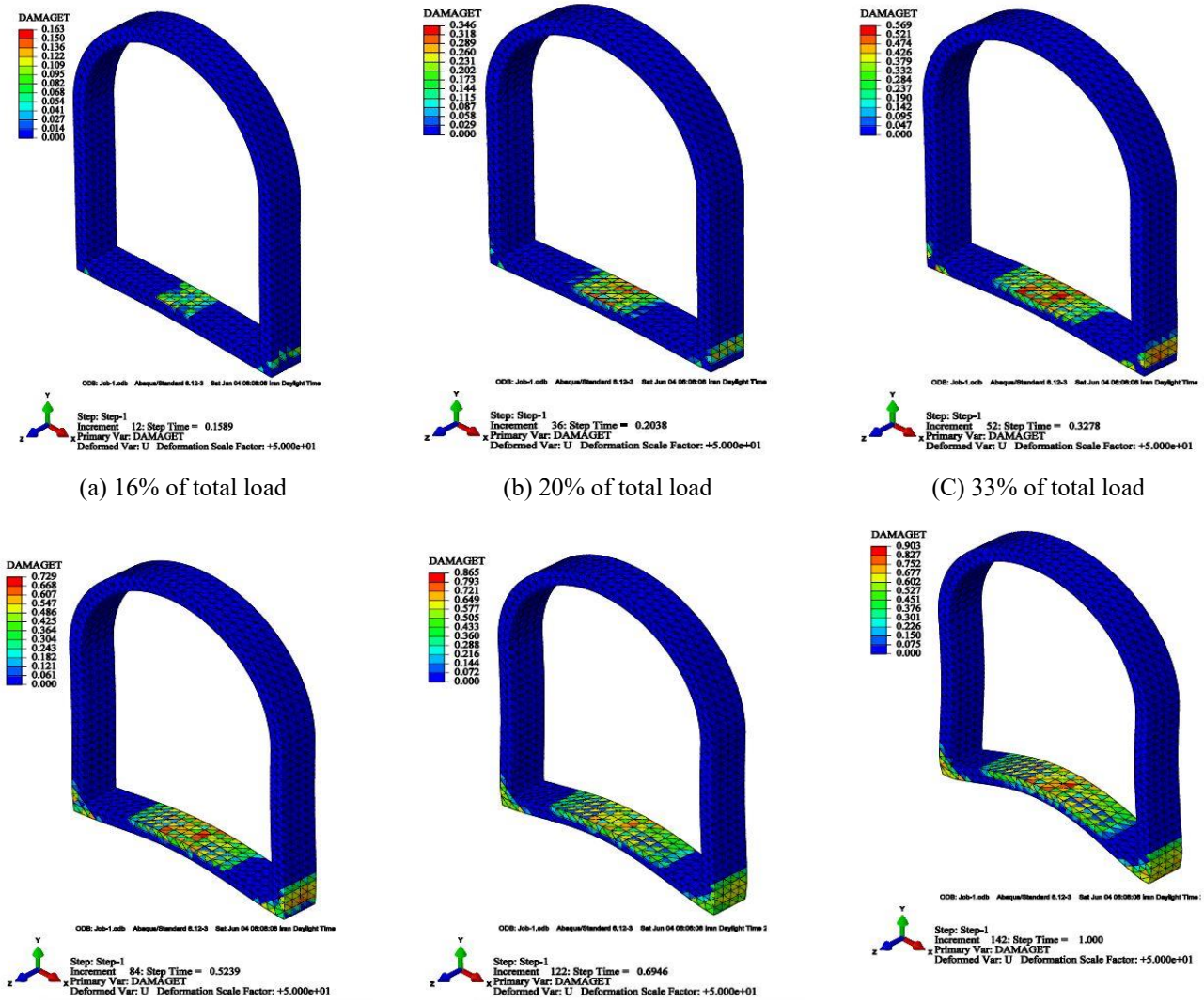

(a) 16% of total load (b) 20% of total load (C) 33% of total load

(d) 52% of total load (e) 69% of total load (f) 100% of total load

Fig. 10 Damage contours of concrete in different stages of loading plus deformation with a scale factor of 50

understood that two sides of the tunnel act as two columns under the traffic loading, experiencing both bending moments and compressive forces. At the end of these columns, the bending moment is maximum; as a result, the damage happens at the corners of the tunnel. Also, the bottom of the tunnel acts as the beam-column element. It is under the bending moment in addition to the compressive force; therefore, more damage occurs in the bottom center of tunnel.

Moreover, to evaluate stress distribution in the reinforcing steels, the von-Mises stress in reinforcing steel of concrete at the end of loading is demonstrated in Fig. 11. Because of the soil load, the bending behavior of two vertical columns (two tunnel sides) and the bottom of the tunnel are toward the tunnel center. Therefore, based on Fig. 11, the maximum stress of reinforcing steels happens at the corners of the concrete box, which is equal to 309 MPa. This amount is less than the yield stress of reinforcing steels, 420 MPa, which means that with this total traffic load, the reinforcing steels did not reach yet to the yielding and plastic states. In the same way, if the traffic load increases, the reinforcing steels surely yield.

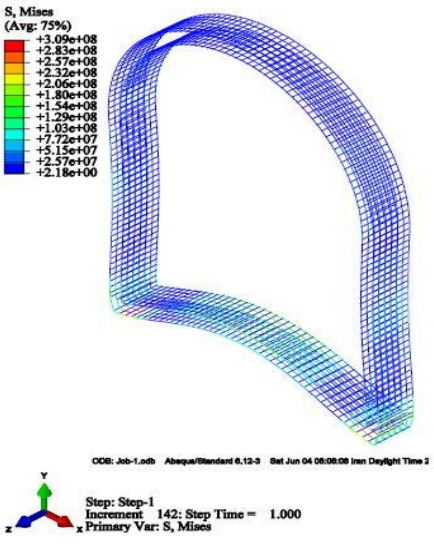

Fig. 11 Von-Mises stress in the reinforcing steels at the end of loading plus deformation with a scale factor of 50

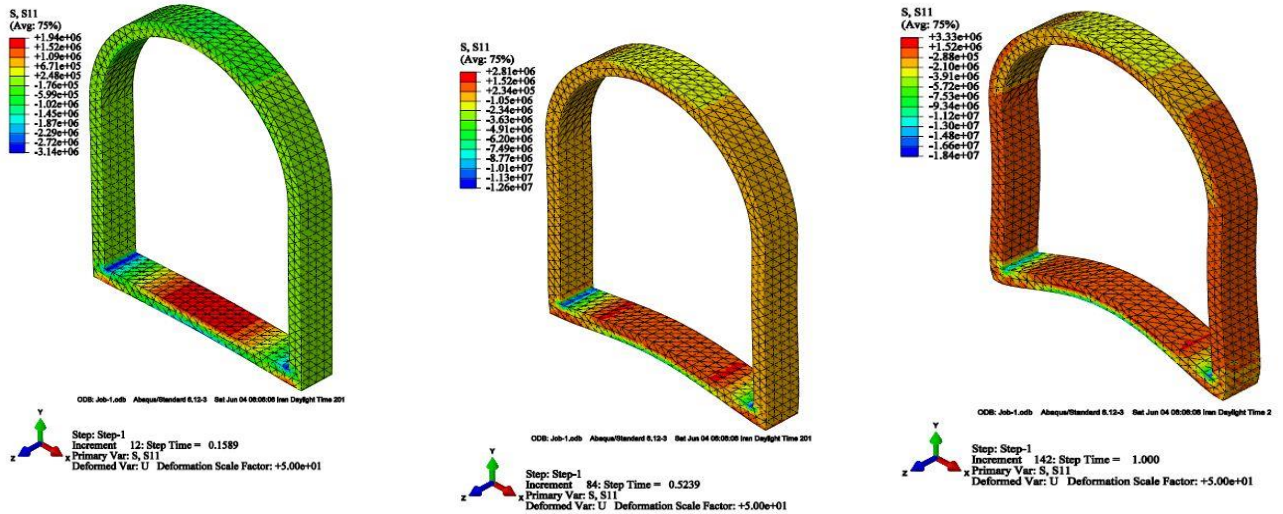

(a) Stress contour 1-1 (16%, 52% and 100% of total load)

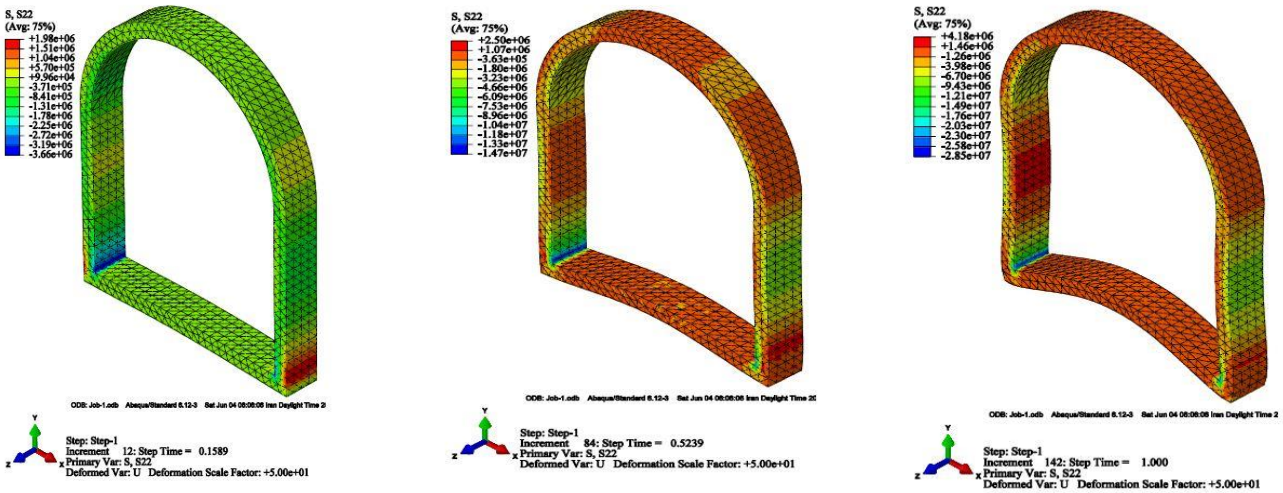

(b) Stress contour 2-2 (16%, 52% and 100% of total load)

Fig. 12 Stress contours in concrete in three stages of traffic loading plus deformation with a scale factor of 50

In order to investigate how the stress distribution in the tunnel, the stress contours 1-1 and 2-2 in the three stages of traffic loading are shown in Fig. 12. In the stress distribution 1-1, observes that stress in the beam is non-uniform and increases with raising the traffic load. The top corners and the bottom center experience compressive loads. In contrast, the bottom corners and the top center experience tensile loads. But, the stress in the columns is uniform in three stages and less than the beam. Nevertheless, the beam (bottom of the tunnel) has a vital role in tunnel response against the traffic load and soil pressure and is the most vulnerable part to damage. In contrast, based on the Fig. 12(b), the stress distribution in the beam and columns is uniform and non-uniform, respectively.

In the following, the effect of traffic load on the cracking and damage analysis of the horseshoe tunnel is discussed. In the same way, with four different loads 20, 50, 100 and 150 KN, nonlinear analysis of the model is performed and the amount of the damage to the tunnel is examined in these cases.

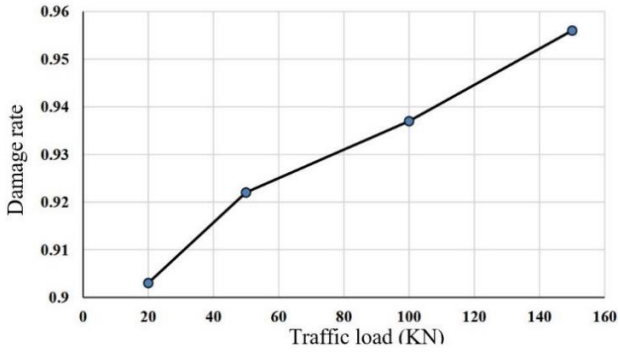

Fig. 13 maximum damages in the tunnel for four different values of traffic load

Fig. 13 shows the trend of the changes in maximum damage in the tunnel for different values of traffic load. It is observed that with increasing the traffic load, the damage in concrete increases, and with increasing 7.5 times the traffic load, the damage rate increases from 0.9 to 0.96.

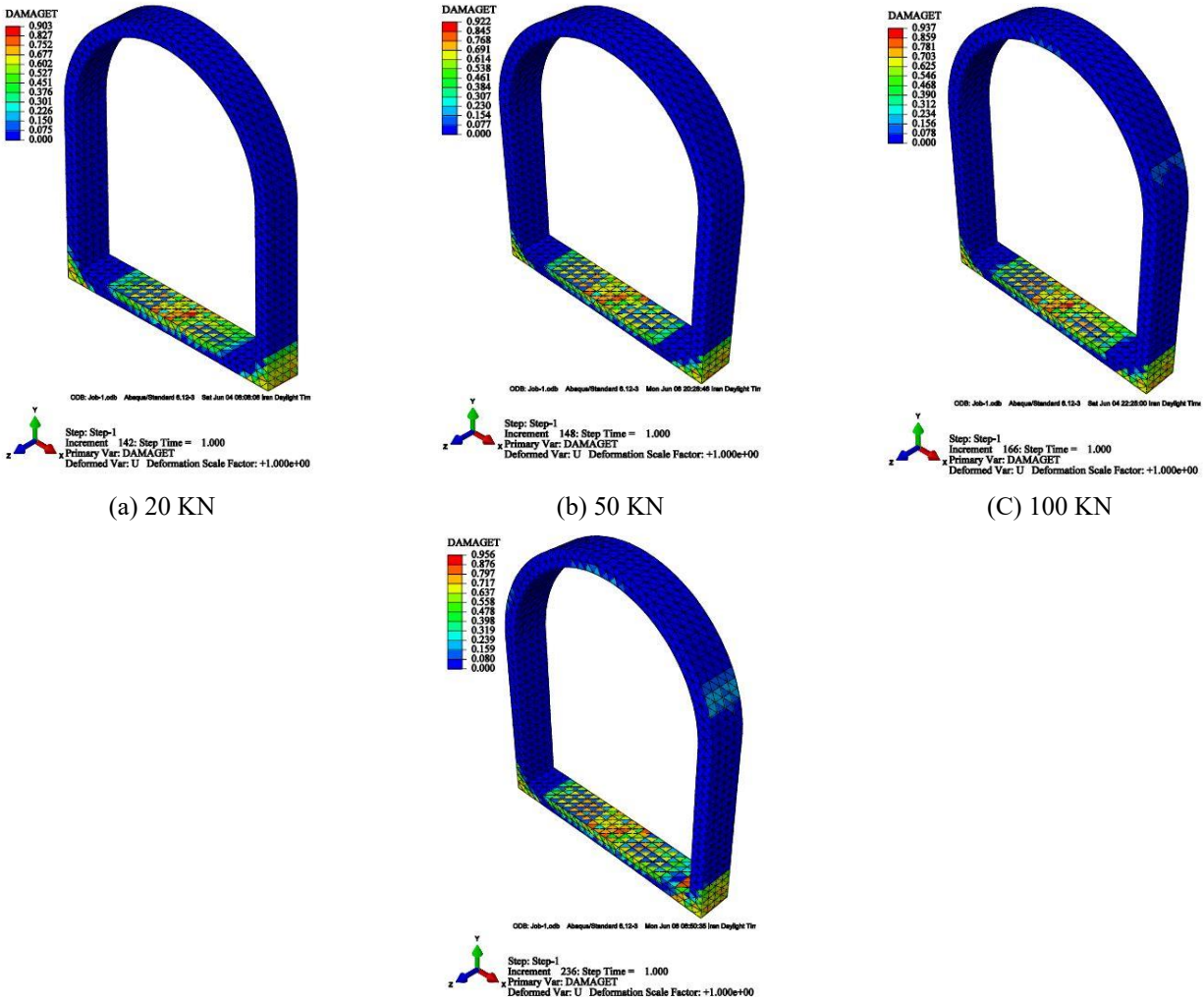

(a) 20 KN (b) 50 KN (C) 100 KN

(d) 150 KN

Fig. 14 Damage contours in the concrete at the end of loading for different values of traffic load

Also, Fig. 14 shows the damage contour in the concrete at the end of traffic loading for different values of traffic load. It can be seen in these four states that damaged areas and damage amount are growing with increasing traffic load. It should be noted that with the increase in the traffic load, the damage is created in the middle of the arc, which naturally increases with the raising in loading.

According to these contours, it can be concluded that in a horseshoe-shaped tunnel, the fracture mechanism is as follows: first, the damage starts at the center of the tunnel bottom. Then, damage and micro-cracks develop at the corners of the tunnel. Eventually, the damage reaches the top of the concrete arch as the loading increases. Therefore, in the design of this tunnel, these critical places should more reinforce to prevent cracking.

5. Conclusions

This paper evaluates the performance of a shallow buried transit tunnel using damage mechanics theory. The tunnel, which has a horseshoe-shaped cross-section, is subjected to soil pressure and traffic loads. Numerical modeling using ABAQUS software was conducted in detail. The study focuses on the cracking phenomenon using the damage plasticity modulus, which accounts for the inelastic behavior of concrete under tension and compression. The analysis identifies the most vulnerable parts of the tunnel, which experience the highest damage due to traffic loads. The main findings are as follows:

- Based on the damage and stress contours in the concrete and steel of the tunnel, the most vulnerable part is the center of the tunnel bottom.
- As soil pressure and traffic load increase, macro-cracks expand in the bottom (beam) and corners (columns) of the tunnel, resulting in more damage.
- The damage value is highest above the center of the tunnel bottom and at the bottom of the tunnel corners. This is because the bending moment and compressive force are greatest in these areas.
- More stress concentration was observed in the reinforcing steel in the corners of the tunnel.

Additionally, unlike the stress 1-1 contour, the stress 2-2 distribution was uniform in the beam and non-uniform in the columns.

- As the traffic load increases, the damage in the concrete also increases. With a 7.5-fold increase in traffic load, the damage rate rose from 0.9 to 0.96.
- The fracture mechanism is as follows: first, the damage starts at the center of the tunnel bottom, then damage and micro-cracks develop at the corners of the tunnel, and eventually, the damage reaches the top of the concrete arch as the loading increases. Therefore, in the design of this tunnel, these critical areas should be reinforced more to prevent cracking.

References

Abdollahipour, A., Marji, M.F., Bafghi, A.Y. and Gholamnejad, J. (2016), "Time-dependent crack propagation in a poroelastic medium using a fully coupled hydromechanical displacement discontinuity method", *Int. J. Fract.*, **199**, 71-87. https://doi.org/10.1007/s10704-016-0095-9.

Acun, B. (2012), *Eurocode 8: Seismic design of buildings, worked examples*, Publications Office of the European Union.

Bassan, S. (2015), "Sight distance and horizontal curve aspects in the design of road tunnels vs. highways", *Tunn. Undergr. Sp. Tech.*, **45**, 214-226. https://doi.org/10.1016/j.tust.2014.10.004.

Bendjebbas, H., Abdellah-ElHadj, A. and Abbas, M. (2016), "Full-scale, wind tunnel and CFD analysis methods of wind loads on heliostats: A review", *Renew. Sust. Energ. Rev.*, **54**, 452-472. https://doi.org/10.1016/j.rser.2015.10.031.

Birtel, V. and Mark, P. (2006), Parameterised finite element modelling of RC beam shear failure. ABAQUS users' conference.

Bryden, P., El Naggar, H. and Valsangkar, A. (2015), "Soil-structure interaction of very flexible pipes: centrifuge and numerical investigations", *Int. J. Geomech.*, **15**(6), 04014091. https://doi.org/10.1061/(ASCE)GM.1943-5622.0000442.

Chen, G.H., Zou, J.F. and Qian, Z.H. (2019), "An improved collapse analysis mechanism for the face stability of shield tunnel in layered soils", *Geomech. Eng.*, **17**(1), 97-107. https://doi.org/10.12989/gae.2019.17.1.097.

Cui, X., Li, S., Lou, J., Wang, Z., Zhang, J., Tang, W. and Gao, Z. (2015), "Dynamic responses and damage analyses of tunnel lining and errant large vehicle during collision", *Tunn. Undergr. Sp. Tech.*, **50**, 1-12. https://doi.org/10.1016/j.tust.2015.05.011.

Falcone, G., Romagnoli, G., Naso, G., Mori, F., Peronace, E. and Moscatelli, M. (2020), "Effect of bedrock stiffness and thickness on numerical simulation of seismic site response. Italian case studies", *Soil Dyn. Earthq. Eng.*, **139**, 106361. https://doi.org/10.1016/j.soildyn.2020.106361.

Haack, A. (2003), Tunnelling in Germany: Statistics (2002/2003), Analysis and Outlook. *TUNNEL-GUTERSLOH*-(8), 14-25.

Haeri, H., Sarfarazi, V., Ebneabbasi, P., Shahbazian, A., Marji, M. F. and Mohamadi, A. (2020), "XFEM and experimental simulation of failure mechanism of non-persistent joints in mortar under compression", *Constr. Build. Mater.*, **236**, 117500. https://doi.org/10.1016/j.conbuildmat.2019.117500.

Hashash, Y.M., Hook, J.J., Schmidt, B., John, I. and Yao, C. (2001), "Seismic design and analysis of underground structures", *Tunn. Undergr. Sp. Tech.*, **16**(4), 247-293. https://doi.org/10.1016/S0886-7798(01)00051-7.

Huang, X., Zhou, Z. and Yang, X. (2018), "Roof failure of shallow tunnel based on simplified stochastic medium theory", *Geomech. Eng.*, **14**(6), 571-580. https://doi.org/10.12989/gae.2018.14.6.571.

Hult, J. (1974), Creep in continua and structures. Topics in Applied Continuum Mechanics: Symposium Vienna, March 1–2, 1974,

Jiang, M. and Yin, Z.Y. (2012), "Analysis of stress redistribution in soil and earth pressure on tunnel lining using the discrete element method", *Tunn. Undergr. Sp. Tech.*, **32**, 251-259. https://doi.org/10.1016/j.tust.2012.06.001.

Kachanov, L. (1986), *Introduction to continuum damage mechanics* (Vol. 10), Springer Science & Business Media.

Kattan, P.I. and Voyiadjis, G.Z. (1990), "A coupled theory of damage mechanics and finite strain elasto-plasticity—I. Damage and elastic deformations", *Int. J. Eng. Sci.*, **28**(5), 421-435. https://doi.org/10.1016/0020-7225(90)90007-6.

Kraus, E., Oh, J. and Fernando, E.G. (2014), "Impact of repeat overweight truck traffic on buried utility facilities", *J. Perform. Constr. Fac.*, **28**(4), 04014004. https://doi.org/10.1061/(ASCE)CF.1943-5509.0000454.

Lee, J. and Fenves, G.L. (1998), "Plastic-damage model for cyclic loading of concrete structures", *J. Eng. Mech.*, **124**(8), 892-900. https://doi.org/10.1061/(ASCE)0733-9399(1998)124:8(892).

LEMAITRE, J. (1971), Evaluation of dissipation and damage in metals submitted to dynamic loading(Constitutive equations for defining dissipation and damage in metals submitted to dynamic loading).

Lemaitre, J. (1984), "How to use damage mechanics", *Nuclear Eng. Design*, **80**(2), 233-245. https://doi.org/10.1016/0029-5493(84)90169-9.

Lemaitre, J. (1986), "Local approach of fracture", *Eng. Fract. Mech.*, **25**(5-6), 523-537. https://doi.org/10.1016/0013-7944(86)90021-4.

Lemaitre, J. and Chaboche, J. (1975), "A non-linear model of creep-fatigue damage cumulation and interaction(for hot metallic structures)", *Mechanics of visco-elastic media and bodies*.

Lemaitre, J. and Dufailly, J. (1987), "Damage measurements", *Eng. Fract. Mech.*, **28**(5-6), 643-661.

Lubliner, J., Oliver, J., Oller, S. and Oñate, E. (1989), "A plastic-damage model for concrete", *Int. J. Solids Struct.*, **25**(3), 299-326. https://doi.org/10.1016/0020-7683(89)90050-4.

Nikadat, N., Fatehi, M. and Abdollahipour, A. (2015), "Numerical modelling of stress analysis around rectangular tunnels with large discontinuities (fault) by a hybridized indirect BEM", *J. Central South Univ.*, **22**, 4291-4299.

Nikadat, N. and Marji, M.F. (2016), "Analysis of stress distribution around tunnels by hybridized FSM and DDM considering the influences of joints parameters", *Geomech. Eng*, **11**(2), 269-288. https://doi.org/10.12989/gae.2016.11.2.269.

Pilkey, W.D. and Pilkey, W.D. (2005), *Formulas for stress, strain, and structural matrices* (Vol. 107). John Wiley & Sons Hoboken, NJ, USA.

Schwer, L. (2014),"Modeling rebar: The forgotten sister in reinforced concrete modeling", *Proceedings of the 13th International LS-DYNA® Users Conference*, https://petergrassl.com/tempFiles/sch14.pdf.

Singh, M., Viladkar, M.N. and Samadhiya, N.K. (2017), "Seismic analysis of Delhi metro underground tunnels", *Indian Geotech. J.*, **47**, 67-83. https://doi.org/10.1007/s40098-016-0203-9.

Struik, L.C.E. (1978), *Physical aging in amorphous polymers and other materials* (Vol. 106). Citeseer. http://resolver.tudelft.nl/uuid:941d2af6-903a-4260-9953-2efb4cb38d2e

Systemes, D. (2011), "Abaqus Analysis User's Manual, Vol. 3: Materials, Version 6.11. *Dassault Systemes Simulia Corp., Providence, RI, USA*.

Trickey, S.A. and Moore, I.D. (2007), "Three-dimensional response of buried pipes under circular surface loading", *J. Geotech. Geoenviron. Eng.*, **133**(2), 219-223.

https://doi.org/10.1061/(ASCE)1090-0241(2007)133:2(219).
Voyiadjis, G.Z. and Kattan, P.I. (1990), "A coupled theory of damage mechanics and finite strain elasto-plasticity—II. Damage and finite strain plasticity", *Int. J. Eng. Sci.*, **28**(6), 505-524.
Voyiadjis, G.Z. and Kattan, P.I. (2005), *Damage mechanics*. CRC Press. https://doi.org/10.1016/0020-7225(90)90053-L.
Wahalathantri, B., Thambiratnam, D., Chan, T. and Fawzia, S. (2011), "A material model for flexural crack simulation in reinforced concrete elements using ABAQUS", *Proceedings of the 1st international conference on engineering, designing and developing the built environment for sustainable wellbeing*, https://eprints.qut.edu.au/41712/1/eddBE2011_260_264_Wahalathantri.pdf.
Wang, G., Lu, W., Yang, G., Yan, P., Chen, M., Zhao, X. and Li, Q. (2020), "A state-of-the-art review on blast resistance and protection of high dams to blast loads", *Int. J. Impact Eng.*, **139**, 103529.
Wang, X., Wang, M., Chen, J., Yan, T., Bao, Y., Chen, J., Qin, P., Li, K., Deng, T. and Yan, G. (2020), "Analysis of calculation of fresh-air demand for road tunnel ventilation design in China", *Tunn. Undergr. Sp. Tech.*, **103**, 103469. https://doi.org/10.1016/j.ijimpeng.2020.103529.
Wang, X. and Zhao, Y. (2006), "Comment on construction of railway tunnels in China by statistical data", *Mod. Tunn. Technol*, **21**, 7-17. https://doi.org/10.1016/j.tust.2020.103469.
Yang, X., Xu, J., Li, Y. and Yan, R. (2016), "Collapse mechanism of tunnel roof considering joined influences of nonlinearity and non-associated flow rule", *Geomech. Eng.*, **10**(1), 21-35. https://doi.org/10.12989/gae.2016.10.1.021.
Yoo, C.S., Chung, S.W., Lee, K.M. and Kim, J.S. (1999), "Interaction between flexible buried pipe and surface load", *J. Korean Geotech. Soc.*, **15**(3), 83-97. https://www.koreascience.or.kr/article/JAKO199911921749210.pdf.
Yoo, C. (2016), "Effect of spatial characteristics of a weak zone on tunnel deformation behavior", *Geomech. Eng.*, **11**(1), 41-58. https://doi.org/10.12989/gae.2016.11.1.041.
Yu, H., Yuan, Y. and Bobet, A. (2017), "Seismic analysis of long tunnels: A review of simplified and unified methods", *Undergr. Sp.*, **2**(2), 73-87. https://doi.org/10.1016/j.undsp.2017.05.003.
Zaid, M. (2021), "Three-dimensional finite element analysis of urban rock tunnel under static loading condition: effect of the rock weathering", *Geomech. Eng.*, **25**(2), 99-109. https://doi.org/10.12989/gae.2021.25.2.099.
Zhao, Y. and Li, P. (2018), "A statistical analysis of China's traffic tunnel development data", https://doi.org/10.1016/j.eng.2017.12.011.

CC